Hereditary paraganglioma : genetics and tumor biology

Hoekstra, A.S.

CHAPTER 3

Parent-of-origin tumorigenesis is mediated by an essential imprinted modifier in SDHD-linked paragangliomas: SLC22A18 and CDKN1C are candidate tumor modifiers

Attje S Hoekstra[1], Ruben D Addie[2,5], Cor Ras[3], Reza M Seifar[3], Claudia A Ruivenkamp[4], Inge H Briaire-de Bruijn[5], Frederik J Hes[4], Jeroen C Jansen[6], Eleonora PM Corssmit[7], Willem E Corver[5], Hans Morreau[5], Judith VMG Bovée[5], Jean-Pierre Bayley[1], Peter Devilee[1,5*]

[1] Department of Human Genetics, Leiden University Medical Center, Leiden, The Netherlands

[2] Center for Proteomics and Metabolomics, Leiden University Medical Center, Leiden, The Netherlands

[3] Department of Biotechnology, Delft University of Technology, Delft, The Netherlands

[4] Department of Clinical Genetics, Leiden University Medical Center, Leiden, The Netherlands

[5] Department of Pathology, Leiden University Medical Center, Leiden 2333 ZC, The Netherlands

[6]Department of Otorhinolaryngology, Leiden University Medical Center, Leiden, The Netherlands

[7]Department of Endocrinology and Metabolic Diseases, Leiden University Medical Center, Leiden, The Netherlands

Accepted in Human Molecular Genetics

Abstract

Mutations in *SDHD* and *SDHAF2* (both located on chromosome 11) give rise to hereditary paraganglioma almost exclusively after paternal transmission of the mutation, and tumors often show loss of the entire maternal copy of chromosome 11. The 'Hensen' model postulates that a tumor modifier gene located on chromosome 11p15, a region known to harbor a cluster of imprinted genes, is essential to tumor formation. We observed decreased protein expression of the 11p15 candidate genes CDKN1C, SLC22A18 and ZNF215 evaluated in 60 *SDHD*-mutated tumors compared to normal carotid body tissue and non-*SDH* mutant tumors.

We then created stable knockdown *in vitro* models, reasoning that the simultaneous knockdown of *SDHD* and a maternally expressed 11p15 modifier gene would enhance paraganglioma-related cellular characteristics compared to *SDHD* knockdown alone. Knockdown of *SDHD* in SNB19 and SHSY5Y cells resulted in the accumulation of succinate, the stabilization of HIF1 protein and a reduction in cell proliferation.

Compared to single knockdown of *SDHD*, knockdown of *SDHD* together with *SLC22A18* or with *CDKN1C* led to small but significant increases in cell proliferation and resistance to apoptosis, and to a gene expression profile closely related to the known transcriptional profile of *SDH*-deficient tumors. Of the 60 *SDHD* tumors investigated, 4 tumors showing retention of chromosome 11 showed SLC22A18 and CDKN1C expression levels comparable to levels in tumors showing loss of chromosome 11, suggesting loss of protein expression despite chromosomal retention.

Our data strongly suggest that *SLC22A18* and/or *CDKN1C* are tumor modifier genes involved in the tumorigenesis of *SDHD*-linked paraganglioma.

Introduction

Hereditary paraganglioma–pheochromocytoma syndrome is characterized by neuroendocrine tumors that originate from both the sympathetic and parasympathetic branches of the autonomic nervous system. Pheochromocytomas (PCC) are generally benign catecholamine-secreting tumors of the adrenal medulla (1), whereas extra-adrenal paragangliomas (EA-PGL) are frequently aggressive tumors that arise in the thorax and abdomen. Paragangliomas of the head and neck (HNPGL) arise most commonly in the carotid body, the main sensor of blood oxygenation, and these highly vascular tumors are often characterized by an indolent, non-invasive growth pattern (2).

Although more than 14 different genes have been linked to PGL/PCC, a subgroup of these genes is associated with hereditary PGL/PCC, including *SDHA* (3), *SDHB* (4), *SDHC* (5), *SDHD* (6), and *SDHAF2* (7). These genes encode subunits of the mitochondrial succinate dehydrogenase (SDH) complex, which plays a central role in the tricarboxylic acid (TCA) cycle and the electron transport chain. In the TCA cycle, SDH converts succinate to fumarate while providing electrons for oxidative phosphorylation in the inner mitochondrial membrane. SDH inactivation results in accumulation of its substrate succinate, which can function as competitor of α-ketoglutarate (α-KG) to broadly inhibit α-KG-dependent dioxygenases leading to HIF activation (8-11). Expression profiling of PGL and PCC shows increased hypoxic-angiogenic expression features and reduced oxidoreductase profiles in *SDH*-deficient tumors compared to non-*SDH* mutant tumors (12;13).

Germline mutations of the *SDHD* and *SDHAF2* genes, unlike mutations of the other *SDH* subunit genes, show a parent-of-origin expression phenotype, with tumor development occurring almost exclusively due to mutations inherited via the paternal line (14;15). Carriers of maternally-inherited mutations develop tumors only very rarely. *SDHD* and *SDHAF2* are both located on the long arm of chromosome 11, whereas the *SDHA, SDHB* and *SDHC* subunit genes are located on chromosome 5 (*SDHA*) or chromosome 1 (*SDHB* and *SDHC*). The 11p15 region of chromosome 11 harbors the main concentration of imprinted genes in the human genome, with 8 genes (Table 1) expressed exclusively from the maternal allele while the opposite allele is silenced by epigenetic mechanisms. Loss of the entire maternal copy of chromosome 11 is a frequent occurrence in *SDHD*-linked paragangliomas (16-18) and since neither *SDHD* nor *SDHAF2* are imprinted, other gene(s) expressed exclusively from the maternal allele must play a role in tumor formation.

Now known as the Hensen model, in 2004 Hensen and colleagues proposed that selective loss of maternal chromosome 11 results in the simultaneous deletion of the *SDHD* gene and an exclusively maternally expressed gene, leading to a parent-of-origin phenotype (Figure 1A) (17). Based on this model, Hensen and colleagues also predicted that, in order to cause disease, a maternally-transmitted *SDHD* mutation would require “mitotic recombination, followed by loss of the recombined paternal chromosome containing the paternal 11q23 region and the maternal 11p15 region” (Figure 1B) (17). This phenomenon has since been observed in at least two cases of maternal inheritance (19;20), strongly supporting the involvement of still unknown maternal genetic factors in tumor formation.

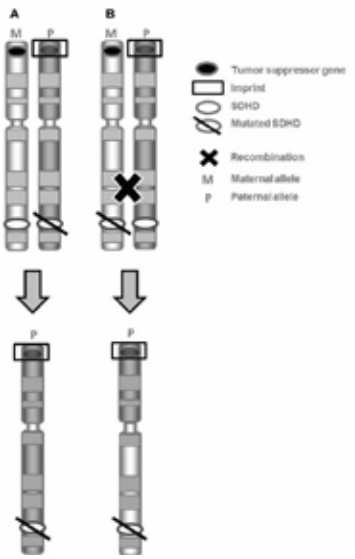

Figure 1. Schematic representation of Hensen model to explain the parent-of-origin effect of *SDHD*-linked paraganglioma. (A) Upon paternal transmission of the *SDHD* mutation and loss of maternal chromosome 11, both the wild type maternal *SDHD* allele and the active tumor suppressor gene located at 11p15 are targeted, thereby initiating tumor formation. (B) In rare cases of maternal transmission of the *SDHD* mutation, at least two events caused by different chromosomal mechanisms will be required to inactivate both the wild type *SDHD* allele and the active maternal tumor suppressor gene, namely loss of the paternal wild type *SDHD* allele by, for example, mitotic recombination, followed by loss of the recombined paternal chromosome containing the paternal 11q23 region and the maternal 11p15 region.

We hypothesized that in a human cell line with two parental copies of chromosome 11, knockdown of *SDHD* together with an additional candidate imprinted gene would lead to a cellular phenotype resembling that of primary paragangliomas. We therefore performed lentiviral stable shRNA knockdown of *SDHD* in SNB19 and SHSY5Y cells, two tumor cell lines of neuroectodermal origin. These cells were then used for additional knockdown of several 11p15 genes, followed by analysis of cell proliferation, apoptosis, TCA cycle metabolites and gene expression profiles. Further (protein/genetics) analysis of candidate tumor modifiers was performed in 60 *SDHD*-mutated tumors. Taken together, our results suggest that *SLC22A18* and *CDKN1C* are potential tumor modifier genes involved in tumor formation of *SDHD*-mutated PGL.

Material and methods

Selection of cell lines

As no human *SDH*-related PGL tumor cell line is currently available, we selected developmentally similar neural crest-derived cell lines. Cell lines carrying somatic mutations in PGL/PCC-linked susceptibility genes, including *VHL* and *MAX* mutations, were excluded based on information from the Catalogue of Somatic Mutations in Cancer (COSMIC) database. SNB19 (glioblastoma) and SHSY5Y (neuroblastoma) cell lines were selected based on a karyotype that demonstrated two copies of chromosome 11. SHSY5Y cells were heterozygous for chromosome 11 as detected by microsatellite markers, while SNB19 cells were homozygous for chromosome 11 (Supplemental Figure 1A). To establish the parental origin of chromosome 11 in the cells, we determined the methylation status of the two imprinted domains at 11p15.5 [H19-differentially methylated region (DMR) and KvDMR]. When both parental copies of chromosome 11 are present, the H19-DMR/KvDMR methylation rate ratio should be around one (39). SHSY5Y cells showed an average methylation rate of 0.75 ± 0.08 for H19-DMR and 0.65 ± 0.1 for KvDMR, resulting in a ratio of 1.1 (Supplemental Figure 1B). The average methylation rate for H19-DMR in SNB19 cells was 0.1 ± 0.1, while the average methylation rate for

KvDMR 0.005 ± 0.03, suggesting loss of imprinting. Nonetheless, clear RNA expression of *H19* (expressed from the maternal allele) and absence of expression of *IGF2* (expressed from the paternal allele) indicated that chromosome 11 in SNB19 cells shows a maternal expression pattern. Both cell lines were therefore considered suitable.

Cell culture

SNB19 cells and HEK293 cells were obtained from DSMZ (ACC 305 and ACC 325, Braunschweig, Germany) and cultured in Dulbecco's Modified Eagle Medium (DMEM, Life Technologies, Paisley, UK) supplemented with 10% fetal bovine serum and penicillin/streptomycin (Life Technologies). SHSY5Y cells were obtained from European Collection of Cell Cultures via Sigma Aldrich (St. Louis, USA, Catalogue no. 86012802). SHSY5Y cells were cultured in DMEM-F12 (Life Technologies, Paisley, UK), supplemented with 15% fetal bovine serum and penicillin/streptomycin, and maintained at 37°C in a humidified atmosphere of 5% CO_2 in air.

Patients and samples

A tissue microarray (25) comprising 100 PGL and 17 PCC paraffin-embedded specimens yielded 5 micrometer sections for immunohistochemistry (IHC). All samples were handled according to the Dutch Code for Proper Secondary Use of Human Materials approved by the Dutch Society of Pathology (www.federa.org). *SDHD* mutant FFPE samples were used for DNA extraction. In addition, we included 8 fresh frozen *SDHD* tumor samples and paired blood samples for DNA extraction. The samples were handled in a coded (pseudonymised) fashion according to procedures agreed with the LUMC ethical board (P12.082).

LOH analysis by microsatellite genotyping

DNA from SNB19 and SHSY5Y cells was isolated using the Wizard Genomic DNA purification kit (Promega, Fitchburg, USA) according to the manufacturer's instructions. Representative tumor areas from FFPE samples were selected to punch 3 cores of 0.6 mm in diameter for DNA isolation. FFPE and fresh frozen tumor sections were incubated overnight with proteinase K at 60°C and DNA was isolated using the Qiagen FFPE DNA kit or QIAamp DNA Mini Kit (Qiagen Benelux B.V., Venlo, The Netherlands), respectively, following manufacturer's instructions. All DNA samples were genotyped for microsatellite markers located on chromosome 11 (primer sequences available upon request). For each marker, thirty nanograms of DNA was amplified over 40 cycles using FastStar Taq DNA Polymerase (Roche). Forward primers were labeled with a 6-FAM, HEX or NED fluorophore (Sigma-Aldrich, St. Louis, MO, USA). Amplicons of microsatellite markers were run on an ABI 3730 genetic analyzer and data were analyzed using Gene Marker software (Soft Genetics, State College, PA 16803, USA), with ABI GeneScan Rox 400 as the internal size standards. LOH of markers in tumor samples was calculated using the allelic imbalance ratio: AIR = (Tumor1/Tumor2)/ (Normal1/Normal2). Tumors were regarded as positive for LOH when the mean allele ratio between tumor and blood was <0.7 for all informative markers, as described earlier (19). In cases where no matching blood DNA sample was available, allele peak ratios were compared to DNA samples with the same or very similar allele combinations. Some markers were either not informative in the patient or did not perform well enough with tumor DNA to give a reliable result and were therefore excluded.

Karyotyping

Conventional cytogenetic analysis on GTG-banded chromosomes from cultured SNB19, HEK293 and SHSY5Y cells was performed according to standard techniques. Briefly, 17 hours before harvesting the cells, 200 µl FdU (5 µM) was added to the cells. Then, the cells were incubated with 200 µl BrdU (14 mg/ml) for another 5-6 hours. Finally, colcemid was added 15 minutes before harvesting and metaphase spreads were prepared according to standard protocols.

Bisulfite-modified PCR and sequencing

DNA (300 ng) from SNB19 and SHSY5Y cells was bisulfite-treated using the EZ DNA methylation kit (Zymo research, Irvine, USA). Bisulfite-treated DNA was then amplified by PCR using primers specific for modified DNA designed with Meth primer (40). Primer sequences for H19 were 5'-GGTTT TAGTGTGAAATTTTTTT-3' (forward) and 5'-CCATAAATATCCTATTCCCAAATAAC-3' (reverse), and 5'-TTGAGGAGTTTTTTGGAGGTT-3' (forward) 5'-ACCC AACCAATACCTCATAC-3' (reverse) for KvDMR1. The PCR program consisted of an initial denaturation step at 94°C for 15 minutes followed by 44 cycles of 20 seconds at 94°C, 30 seconds at 55°C for KvDMR1 and 52.5°C for H19, followed by 5 minutes at 72°C. Sanger sequencing of PCR products was performed using standard protocols, and methylation rates were evaluated using ESME software (41).

CDKN1C and *SLC22A18* mutation analysis

All exons of the *CDKN1C* and *SLC22A18* genes were amplified by PCR (primer sequences available on request). Twenty nanograms of genomic DNA and matched normal DNA from 6 *SDHD*-linked patients was amplified and primer annealing was performed at 58°C. PCR fragments were purified using the Nucleospin gel and PCR clean-up kit (Macherey-Nagel). Sequencing was performed using standard protocols and data were analyzed using Mutation Surveyor software (Softgenetics).

Tissue samples and immunohistochemistry

FFPE tissue samples used for IHC were as described in 'patients and samples'. As control tissue, whole sections of 4 normal carotid bodies were included, obtained from anonymous patients at autopsy within 24 hours after death. We reviewed the histological appearance of all samples (JVMGB, JPB, ASH) and confirmed diagnoses by routine IHC staining for S-100 (detecting sustentacular cells) and chromogranin A (detecting chief cells). Mutation detection was confirmed by routine SDHA and SDHB immunohistochemical staining, as described previously (30).

Primary antibodies for IHC analysis were used as follows: Rabbit polyclonal antibody for detection of SLC22A18 (1:3200, Proteintech), KCNQ1 (1:100, Sigma Aldrich), PHLDA2 (1:200, Abcam), CDKN1C (1:1600, Sigma Aldrich), ZNF215 (1:200, Sigma Aldrich). Placenta and liver were used as a positive control. After antigen retrieval by exposure to microwave heating in citrate buffer, pH 6.0 at 100°C for 10 min, sections were blocked for 30 min with 10% goat serum and incubated overnight at 4°C with primary antibodies. Signal detection was performed with Envision+ (DAKO, Agilent Technologies, Belgium) and the chromogen 3,3'-diaminobenzidine according to manufacturer's instructions. The results of the immunohistochemical labeling were scored semi-quantitatively: the intensity of labeling was assessed on a scale of 0 to 3 (0 = none; 1 = weak; 2 = moderate; 3 = strong), and the percentage of positive cells was assessed on a scale of 0 to 4 (0 = 0% positive; 1 = 1-24% positive; 2 = 25-49% positive; 3 = 50-74%; 4 = 75-100% positive cells). The two scores were then

added to reach a total sum score ranging from 0-7. The scoring was performed independently by two observers blinded for clinicopathological data (ASH and JVMGB) and discrepancies were discussed. Photos of IHC sections were obtained using a Leica DFC550 camera and the Leica Application Suite, software version 4.5 (Heerbrugg, Switzerland).

Gene knockdown

To create stable cell lines with a single or double knockdown of genes, four validated MISSION® shRNA constructs and one non-validated MISSION® shRNA construct (TRCN0000231553 -237878, -147951, -344525 and -13054) targeting human *SDHD* (NM_003002.1), *CDKN1C* (NM_000076), *OSBPL5* (NM_020896), *SLC22A18* (NM_002555) and *ZNF215* (NM_013250), respectively (Sigma Aldrich, St. Louis, USA) or a scrambled shRNA encoding plasmid (SHC002 Sigma Aldrich) were used to produce infectious virus particles. To evaluate the transduction efficiency, the MISSION TurboGFP control plasmid (SHC003 Sigma Aldrich) was used. HEK293T cells were transfected with the shRNA constructs together with helper plasmids encoding HIV-1 gag-pol, HIV-1 rev, and the VSV-G envelope as described (42). Viral supernatants were added to SNB19, HEK293 and SHSY5Y cells in fresh medium supplemented with 8 µg/ml Polybrene (Sigma Aldrich) and the cells were incubated overnight. The next day, the medium was replaced with fresh medium. Selection was carried out using 2 µg/ml puromycin. Transduction efficiency was analyzed 3 to 6 days post transduction. Experiments were performed 2-3 and 4-5 weeks after transduction of cells with shRNAs.

RT-PCR analysis

Total RNA from cells was isolated using the Nucleospin RNA II kit (Macherey-Nagel, Düren, Germany) according to manufacturer's instructions. cDNA was synthesized from 1µg RNA using the Omniscript RT kit (Qiagen, Venlo, Netherlands). Gene expression was determined using quantitative PCR and was measured in triplicate on the CFX96 Real-Time System (Bio-Rad, USA) using the iQ SYBR Green Supermix (Biorad, California, USA). The relative quantification of target mRNA was performed by the $2^{-\Delta\Delta CT}$ method (43). Results from the housekeeping genes *HNRMP*, *TBP* and *HPRT* were used as references. Target genes were *SDHD, CDKN1C, SLC22A18*, *OSBPL5, ZNF215, GLUT1, EGLN3, BNIP3, ENO1* and *VEGF*.

Western blotting

Total protein was isolated using RIPA buffer (Sigma Aldrich) supplemented with "complete" protease inhibitor cocktail (Roche, Germany). The concentration of protein was determined by bicinchoninic acid protein assay (Thermo Scientific Pierce, Rockford, USA). Equal amounts of protein (35 µg) were separated by SDS-PAGE and transferred onto polyvinylidene fluoride (PVDF) membranes (Millipore). After blocking with 5% (w/v) non-fat milk powder, membranes were incubated overnight at 4 °C with the following antibodies: SDHB (Sigma Aldrich) and HIF-1α (Novus Biologicals, Littleton, USA) in a dilution of 1:500 in blocking buffer (Rockland, Gilbertsville, USA). α-tubulin was used as a loading control (1:2000, Sigma Aldrich). Visualization and quantification was carried out using the LI-COR Odyssey® scanner (Bad Homburg, Germany) and software (LI-COR Biosciences).

Microarray expression analysis

Quality control, RNA labeling, hybridization and data extraction were performed at ServiceXS B.V. (Leiden, The Netherlands). RNA concentrations were measured using the Nanodrop ND-1000

spectrophotometer (Nanodrop Technologies, Wilmington, DE, USA). The RNA quality and integrity was determined using Lab-on-a-Chip analysis on the Agilent 2100 Bioanalyzer (Agilent Technologies, Inc., Santa Clara, CA, USA). Biotinylated cRNA was prepared using the Illumina TotalPrep RNA Amplification Kit (Ambion, Inc., Austin, TX, USA) according to the manufacturer's specifications with an input of 200 ng total RNA. Per sample, 750 ng of the obtained biotinylated cRNA samples was hybridized to the Illumina HumanHT-12 v4 BeadChip (Illumina, Inc., San Diego, CA, USA). Hybridization and washing were performed according to the Illumina Manual "Direct Hybridization Assay Guide". Scanning was performed on the Illumina iScan (Illumina, Inc., San Diego, CA, USA). Image analysis and extraction of raw expression data was performed with Illumina GenomeStudio v2011.1 Gene Expression software.

Bioinformatic analysis

Normalization and quality control was performed using the Bioconductor "lumi" package of R (lumi) (44). Samples were clustered using an unsupervised hierarchical clustering method to delineate groups with biological distinction. The R package 'Linear Models for Microarray Data' (LIMMA) was used for the assessment of differential expression of individual genes between the different subgroups (45). Overall gene expression differences between scrambled control and *SDHD* knockdown, scrambled control and *SDHD+CDKN1C* knockdown or scrambled control and *SDHD+SLC22A18* knockdown subgroups in SNB19 and SHSY5Y cells were evaluated with the 'global test' designed by J.J. Goeman using the R package 'global test' available on Bioconductor (46). We applied the global test in order to evaluate subtle differences between the different subgroups, as this test has greater power to detect gene sets with small effect sizes (46;47). We performed a pathway-based analysis using the global test on pathways described in the publicly available pathway database Kyoto Encyclopedia of Genes and Genomes (KEGG) annotations (48). KEGG pathway analysis of scrambled control HEK293 cells versus *SDHD* knockdown was not consistent with tumor gene expression profiles of PGL with *SDH* gene mutations (12;49) and was therefore excluded as a relevant model. All tests, both for genes and pathways, were corrected for multiple testing based on the false discovery rate (FDR) criterion, using the Benjamini and Hochberg method (50). Comparison analysis and functional categorization of the different subgroups was performed with Ingenuity Pathway Analysis (IPA; www.ingenuity.com). All data are available at the GEO database (GSE80968).

Cellular DNA content and flow cytometry

Using the Vindelov technique (51), DNA staining was performed as follows: Cells were centrifuged (500g, 5 min) and washed in PBS, then 300 µl of solution A containing trypsin (0.3 g/L, Sigma) at pH 7.6 was added and incubated for 2 hours at 37°C. Next, 225 µl of solution B containing RNAse (0.5g/L, Sigma) and a trypsin inhibitor (0.1 g/L Sigma) was added, followed by a 10 min incubation at room temperature (RT). Finally, a third incubation at RT was carried out for at least 15 min after the addition of 225 µl of propidium iodide (PI) (0.42g/L, Sigma) (solution C). Samples were measured using an LSRII (BD Biosciences, Erembodegem, Belgium) flow cytometer. Detector D (BP610/20 nm) was used to collect PI fluorescence. The WinList 8.0 and ModFit 4.0.1 software packages (Verity Software House, Inc., Topsham, ME) were used for data analysis.

xCelligence

The RTCA xCelligence system (Roche Applied Sciences, Almere, the Netherlands), based on cell electrode substract impedance detection technology, was used for proliferation assays. Cell lines were plated at a density of 10.000 cells per well in a 16-well E-Plate. The plates were loaded into the RTCA station in the cell culture incubator immediately after plating and cell index was acquired every 30 min. Experiments were performed in triplicate.

Assessment of apoptosis

SNB19 and SHSY5Y cells were stimulated with 2, 4 or 8 µM staurosporine (Sigma) or with 10, 20 or 40 µM cisplatin (Sigma). The ApoLive-Glo multiplex Assay (Promega, Madison, USA) was used to measure cell viability and apoptosis in the same sample following the manufacturer's protocol. Briefly, the viability is measured by the activity of a protease marker of cell viability. Apoptosis is measured by the addition of a luminogenic caspase-3/7 substrate (Caspase-Glo 3/7) which is cleaved in apoptotic cells to produce a luminescent signal. Fluorescence at 400 Ex/505 Em (viability) and luminescence (apoptosis) were measured with a Victor 3 machine (PerkinElmer, Massachusetts, USA).

Nuclear fragmentation was determined in SNB19 and SHSY5Y cells stimulated with 4 µM staurosporine. Cells were fixed with 4% paraformaldehyde for 15 min. Then, the cells were washed three times in PBS and stained with 50 µg/ml 4,6-diamidino-2-phenylindole-2-HCl (DAPI; Sigma) in Vectashield mounting medium under a cover slip. Images of fixed cells were acquired on a Zeiss Axio Imager M2 fluorescence microscope equipped with an HXP 120 metal-halide lamp used for excitation. Fluorescent probes were detected using the following filters: DAPI (excitation filter: 350/50 nm) and GFP (excitation filter: 470/40 nm). Images were recorded using ZEN 2012 software.

TCA cycle metabolite quantification by LC-MS/MS

Sample preparation for biochemical analysis of SNB19 and SHSY5Y cells was performed according to (52), using ice cold 90% MeOH: $CHCl_3$ as extraction solvent containing ^{13}C-labeled isotopes of nucleotides as internal standards. Dried samples were reconstituted in 100µl H_2O for compatibility with the liquid chromatography-tandem mass spectrometry (LC-MS/MS) method (53). The concentrations of citric acid, α-ketoglutarate, succinate, fumarate and malate were determined by anion-exchange LC-MS/MS. The concentrations of AMP, ADP and ATP were determined by ion-pair reverse-phase LC-MS/MS (54).

Statistical analysis

IBM SPSS Statistics 20.0 for Windows software package (SPSS, Armonk, NY: IBM Corp) was used to analyze the results. The statistically significance of differences between 2 groups was assessed by the Mann-Whitney U test, and the 1-way analysis of variance test was used for comparisons of more than 2 groups. $P<0.05$ was considered statistically significant.

Results

Protein expression of chromosome 11p15 candidate genes in SDHD mutant PGL

We selected imprinted 11p15 candidate modifier genes reasoning that a gene of interest would be expressed in normal carotid body tissue and lost in *SDHD* mutant tumors. Using immunohistochemistry (IHC), we analyzed the protein expression of specific 11p15 genes (indicated in bold in Table 1) in normal human post-mortem carotid bodies, *SDHD*-related tumors and non-*SDH* mutant PCCs. Expression of SLC22A18 was significantly decreased in the chief cell, the neoplastic cell population, of *SDHD* mutant tumors, while remaining abundant in all normal carotid bodies and non-*SDH* mutant tumors (Fig. 2A-D). ZNF215 showed no or low expression (score 0-2) in chief cells in 85% of *SDHD*-related tumors, and expression was significantly lower compared to normal carotid bodies (Fig. 2A, E-G). The nuclear expression of CDKN1C was very low in the normal carotid body and absent in *SDHD* mutant PGL (Fig. 2A, 2H-I). However, CDKN1C was expressed in non-*SDH* mutant tumors (Fig. 2A, 2J). By contrast, KCNQ1 and PHLDA2 were expressed in *SDHD* mutant tumors (Fig. 2A, 2K-O), effectively excluding them as candidates.

Table 1. Imprinted genes expressed exclusively from the maternal allele on 11p15

Gene	Chromosome location	Description	Expressed allele	Imprinted allele
KCNQ1DN	11p15.4	non-coding RNA	Maternal	Paternal
ZNF215	11p15.4	zinc finger protein 15	Maternal	Paternal
OSBPL5	11p15.4	member oxysterol-binding protein family	Maternal	Paternal
PHLDA2	11p15.5	pleckstrin homology-like domain family A member 2	Maternal	Paternal
CDKN1C	11p15.5	cyclin-dependent kinase inhibitor 1c	Maternal	Paternal
H19	11p15.5	non-coding RNA	Maternal	Paternal
KCNQ1	11p15.5	encoding voltage-gated potassium channel	Maternal	Paternal
SLC22A18	11p15.5	poly-specific organic cation transporter	Maternal	Paternal

Bold indicates the candidate genes investigated in this study.

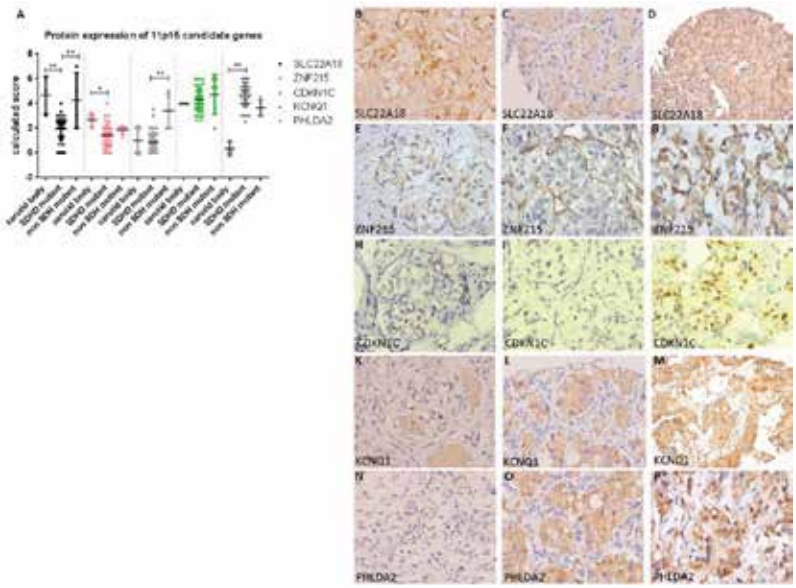

Figure 2. Protein expression in normal human carotid bodies, *SDHD* and non-*SDH* mutant tumors. (A) Dot plot showing immunohistochemical expression levels of SLC22A18, CDKN1C, ZNF215, KCNQ1, and PHLDA2 in normal carotid bodies, *SDHD* and non-*SDH* mutant tumors. Data are represented as calculated mean score ± standard deviation. *p< 0.05; **p<0.001. Representative staining data (40x magnification) show strong nuclear immunostaining of (B) SLC22A18 protein in chief cells in normal carotid bodies, whereas the nuclear tumor cell staining was lost in (C) *SDHD* mutant tumors. (D) SLC22A18 is expressed in non-*SDH* mutant tumors. (E) Expression of ZNF215 is present in the chief cell compartment of normal carotid body, but is absent in (F) *SDHD*-mutated tumors. (G) Low expression of ZNF215 is observed in non-*SDH* mutant tumors. (H) Very low nuclear expression of CDKN1C was observed in chief cells of normal carotid bodies and was absent in (I) *SDHD*-mutated tumors. (J) CDKN1C is highly expressed in non-*SDH* mutant tumors. (K) Cytoplasmic expression of KCNQ1 was observed in normal carotid bodies, (L) *SDHD* mutant tumors, and (M) non-*SDH* mutant tumors. (N) Cytoplasmic expression of PHLDA2 was present in normal carotid bodies and (O) *SDHD* mutant tumors, and (P) non-*SDH* mutant tumors.

SDHD knockdown leads to succinate accumulation, reduced ATP levels and HIF activation

In order to evaluate metabolic changes and HIF1 activation induced by loss of *SDHD*, we generated subclones of SNB19 and SHSY5Y cells with stable knockdown of *SDHD*. Knockdown of *SDHD* was confirmed by real-time analysis of RNA expression levels and by immunoblotting (Fig. 3A), with decreased SDHB protein levels taken as a marker for SDH deficiency (21). As expected (11), suppression of *SDHD* resulted in the significant accumulation of succinate in both SNB19 and SHSY5Y cells (Fig. 3B). In addition, ATP levels were also significantly decreased (Fig. 3C). Suppression of *SDHD* expression increased HIF1α protein levels (Fig. 3D) as well as mRNA expression of HIF1 target genes by at least 2 fold, including glucose transporter 1 (GLUT1), Bcl-2-like 19kDa-interacting protein 3 (BNIP3), prolyl hydroxylase 3 (EGLN3), enolase 1 (ENO1) and vascular endothelial growth factor (VEGF) compared to scrambled control cells (Fig. 3E).

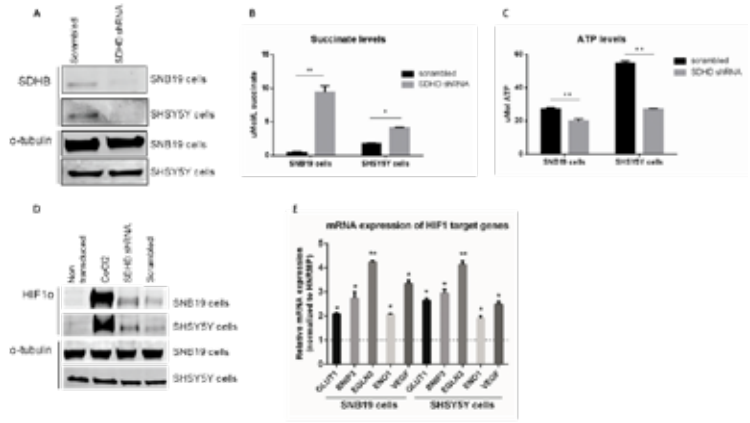

Figure 3. *SDHD* knockdown leads to accumulation of succinate, reduction in ATP levels and HIF1 stabilization. (A) SNB19 and SHSY5Y cells with stable knockdown of *SDHD* demonstrate decreased SDHB protein levels in total protein extract compared to control cells (scrambled shRNA). α-Tubulin was used as a loading control. (B) Succinate levels quantified by LC/MS/MS were increased in SNB19 and SHSY5Y cells with stable knockdown of *SDHD* compared to scrambled control cells. (C) ATP levels as quantified by LC/MS/MS were decreased in SNB19 and SHSY5Y cells with stable knockdown of *SDHD* compared to scrambled control cells. (D,E) HIF1α levels were assessed in total protein extract by western blotting. α-Tubulin was used as a loading control. Stimulation with 200μM $CoCl_2$ for 24 hours was used to induce HIF1 stabilization. Knockdown of *SDHD* resulted in stabilization of HIF1α protein and (B) increased mRNA expression of HIF1 target genes, including GLUT1, BNIP3, EGLN3, ENO1 and VEGF, compared to control (dashed line), as measured by RT-PCR. mRNA expression of *SDHD* knockdown cells was normalized to control cells (scrambled shRNA), indicated by the dashed line. HNRMP was used as a housekeeping gene. Error bars represent standard deviation for duplicate experiments. *p<0.05, **p<0.01.

To study the effects of 11p15 candidate gene loss in *SDHD* knockdown cells, we carried out additional knockdown of *OSBPL5, SLC22A18, CDKN1C* or *ZNF215* in both SNB19 and SHSY5Y cells. Stable knockdown of each gene was confirmed by real-time analysis of RNA expression levels (Supplementary Fig. 2). Cells with double knockdown of *SDHD* and either *SLC22A18*, *CDKN1C* or *OSBPL5* exhibited succinate levels equivalent to single knockdowns of *SDHD*, while combined knockdown of *SDHD* and *ZNF215* resulted in a small (non-significant) reduction in succinate levels (Figs. 4A and 4B). Consistent with these findings, the ratio of succinate to fumarate was increased in cells with single knockdown of *SDHD* compared to scrambled control cells and did not change significantly following additional knockdown of either *SLC22A18*, *CDKN1C*, *OSBPL5* or *ZNF215* (Fig 4C-D). Furthermore, the elevated succinate/α-KG ratio following *SDHD* knockdown did not change significantly upon additional knockdown of any candidate gene (Fig. 4E-F).

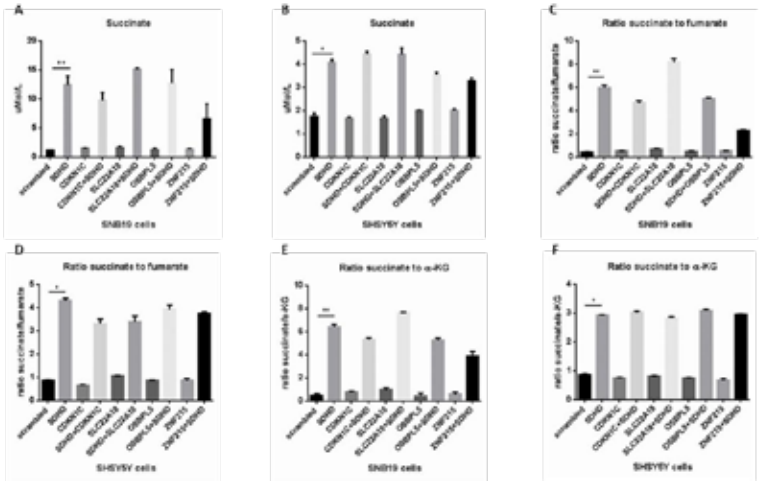

Figure 4. No metabolic changes by stable knockdown of *SDHD* and 11p15 genes. (A,B) Increased succinate levels following stable knockdown of *SDHD* did not change significantly in *CDKN1C, SLC22A18* or *OSBPL5* double knockdown SNB19 or SHSY5Y cells, as quantified by LC/MS/MS. (C,D) The ratio of succinate to fumarate and (E,F) succinate to α-KG is not increased in cells with double knockdowns of *CDKN1C, SLC22A18*, *OSBPL5* or *ZNF215* compared to *SDHD* knockdown, as quantified by LC/MS/MS. Error bars represent standard deviation for duplicate experiments. *p<0.05, **p<0.01.

Increased cell proliferation following SDHD and CDKN1C or SLC22A18 double knockdown

HNPGL is characterized by unusually slow growth, with a reported doubling time of 4 years (2). Using a real-time cell proliferation system, *SDHD* knockdown in SHSY5Y resulted in reduced proliferation (Fig. 5A) and a lower S-phase fraction (Fig. 5B), relative to controls. However, reduced proliferation could not be attributed to cell cycle arrest at G2/M, since no changes were found in the G2/M fraction in *SDHD* knockdown compared to control cells (Fig. 5B).

However, a significantly increased rate of cell proliferation was seen following double knockdown of *SDHD* and *CDKN1C* (Fig. 5C), or of *SDHD* and *SLC22A18* (Fig. 5D), compared to single knockdown of *SDHD*. By contrast, knockdown of *SDHD* together with *OSBPL5* (Fig. 5E) or *ZNF215* (Fig. 5F) did not result in enhanced proliferation compared to single knockdown of *SDHD*. Only very minor changes in cell proliferation were observed in SNB19 cells, perhaps because these cells show much faster intrinsic growth compared to SHSY5Y cells.

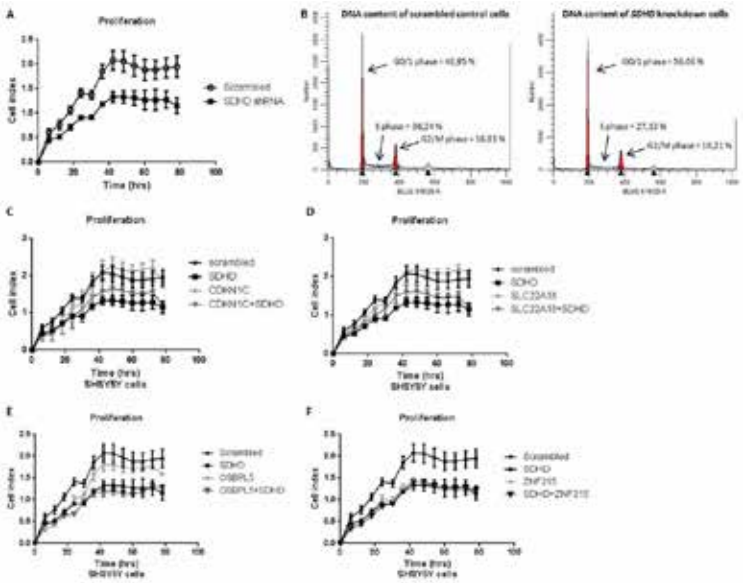

Figure 5. Increased cell proliferation in cells with knockdown of *SDHD* and *CDKN1C* or *SLC22A18*. (A) SHSY5Y cells with stable knockdown of *SDHD* demonstrate a reduced cell proliferation compared to scrambled control cells, measured in real-time using xCelligence. (B) Using propidium iodide and FACS analysis, DNA content histograms showed a decreased S phase fraction and increased G0/1 fraction in *SDHD* knockdown cells compared to scrambled cells. The acquired FACS data were analyzed by ModFit LT software (Verity Software House, Inc.). (C) Using xCelligence, SHSY5Y cells with stable knockdown of *SDHD* and *CDKN1C* or (D) *SLC22A18* show increased proliferation compared to single knockdown of *SDHD*. (E) No differences in cell proliferation were observed when comparing single knockdown of *SDHD* to combined knockdown of *SDHD* and *OSBPL5* or (F) *SDHD* and *ZNF215*.

Knockdown of SDHD and SLC22A18 results in apoptosis resistance

No significant apoptotic activity has been detected in HNPGLs, suggesting that apoptotic mechanisms may be impaired or blocked (22). Using *SDHD* knockdown SHSY5Y cells, we induced apoptosis using various concentrations of staurosporine or cisplatin and studied key features of apoptosis such as nuclear fragmentation and activation of caspase 3/7. Staurosporine was significantly less proficient in inducing apoptosis upon *SDHD* knockdown (Figure 6A), and SNB19 cells showed similar results, but with lower overall sensitivity to apoptosis (Fig. 6B). *SDHD* knockdown also resulted in resistance to cisplatin-induced apoptosis, compared to control cells (Fig. 6C). Induction of apoptosis using staurosporine or cisplatin was also accompanied by decreased cell viability (Fig. 6D). Only one candidate gene showed significant differences in apoptosis resistance following double knockdown, *SLC22A18*. In SNB19 cells the combined knockdown of *SDHD* and *SLC22A18* resulted in significant apoptosis resistance compared to single knockdown of *SDHD* (Fig. 6F).

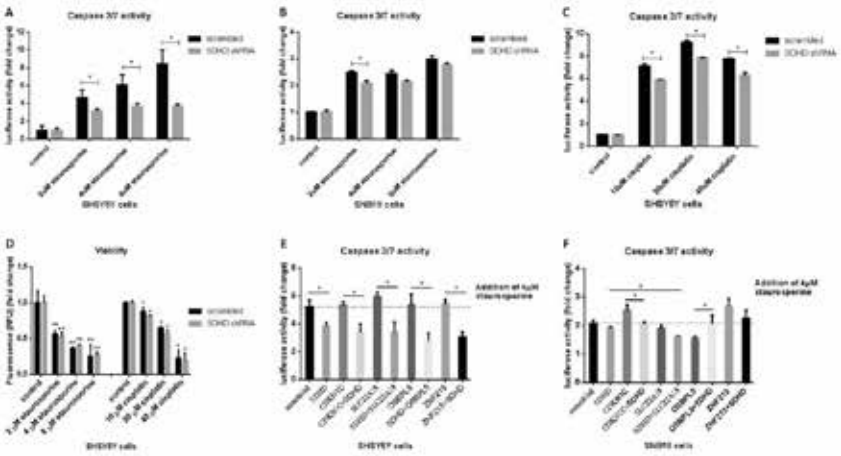

Figure 6. Knockdown of *SDHD* together with *SLC22A18* results in apoptosis resistance. (A) Apoptosis was induced with 2μM, 4μM or 8μM staurosporine for 2 hours in SHSY5Y cells and caspase 3/7 activity was measured using the APOLive-GLO Multiplex Assay (Promega). (B) Apoptosis was induced in SNB19 cells following exposure to 2μM, 4μM or 8μM staurosporine (for 24 hours). SNB19 cells showed lower sensitivity to apoptosis induction than SHSY5Y cells. (C) SHSY5Y cells were exposed to 10μM, 20μM or 40μM cisplatin for 18 hours. (D) Cell viability is decreased by the addition of 2μM, 4μM and 8μM staurosporine or 10μM, 20μM and 40μM cisplatin, measured by APOLive-GLO Multiplex Assay. (E) Using 4μM staurosporine for 2 hours, apoptosis was induced in SHSY5Y cells and double knockdown cells were analyzed. Silencing of *SDHD* together with *CDKN1C, SLC22A18, OSBPL5* or *ZNF215* resulted in small but non-significant decreases in apoptosis compared to *SDHD* knockdown alone. (F) Apoptosis was induced by 4μM staurosporine for 24 hours in SNB19 cells. Double knockdown of *SDHD* and *SLC22A18* led to a small but significant reduction in apoptosis compared to knockdown of *SDHD* alone. Error bars represent standard deviation for duplicate experiments. *p<0.05, **p<0.01.

Gene expression changes characteristic for SDH-related PGL/PCC by the combined loss of SDHD and SLC22A18 or CDKN1C

SDHD PGLs display distinctive gene expression patterns compared to paragangliomas and pheochromocytomas linked to other genes. Unsupervised hierarchical cluster analysis of gene expression in SNB19 and SHSY5Y cells showed that while cell type is the primary determinant of clustering (Supplemental Figure 3), a large number of genes are significantly differentially expressed in both SNB19 cells and SHSY5Y cells depending on single *SDHD*, or double knockdown together with *SLC22A18* or *CDKN1C*. Focusing on pathways believed to play a role in PGL/PCC (12;13) and exploiting the pathway database KEGG, we selected functional gene sets for analysis, including oxidative phosphorylation, citrate cycle (TCA cycle), apoptosis, glycolysis, VEGF signaling pathway, pathways in cancer including HIF, glutathione metabolism and beta-alanine metabolism.

Analysis using the global test revealed a synchronized suppression of mitochondrial functions in *SDHD* knockdown SNB19 cells compared to scrambled control cells, characterized by significant differential expression of components of the oxidative response and TCA cycle (Table 2). Interestingly, double knockdown of *SDHD* together with either *CDKN1C* or *SLC22A18* in SNB19 cells led to greater (significant) differential expression of additional PGL/PCC-associated pathways (Table

2). These changes were not observed in SHSY5Y cells using the global test (Supplemental Figure 3). To identify further cellular functions that might be affected by the observed gene expression changes, we performed a series of comparisons using Ingenuity Pathway Analysis (IPA). This analysis revealed that double knockdown of *SDHD* and *SLC22A18* or of *SDHD* and *CDKN1C* strongly decreased apoptosis and cell death-associated gene expression in both SNB19 cells (Fig. 7A) and SHSY5Y cells (Fig. 7B), compared to single *SDHD* knockdown. In addition, both double knockdowns induced gene expression signatures for increased cell proliferation and cell survival compared to single *SDHD* knockdown.

Table 2. Global test of KEGG pathways in three SNB19 cell subgroups

Pathway ID	KEGG pathway name	Number of genes	P-value Control vs SDHD shRNA	P-value Control vs SDHD + CDKN1C shRNA	P-value Control vs SDHD + SLC22A18 shRNA
00190	Oxidative phosphorylation	158	0,002	0,001	0,005
00020	Citrate cycle	50	0,002	0,0005	0,01
00410	beta-Alanine metabolism	34	0,05	0,04	0,01
04210	Apoptosis	151	0,1	0,00002	0,003
00480	Glutathione metabolism	83	0,9	0,1	0,01
00010	Glycolysis	122	0,9	0,5	0,5
05200	Pathways in cancer	601	1	0,008	0,05
04370	VEGF signaling pathway	130	1	0,2	0,1

Number of genes indicates the number of genes involved in the KEGG pathway. P-value is corrected for multiple testing using Benjamini–Hochberg, as described in Material and Methods.

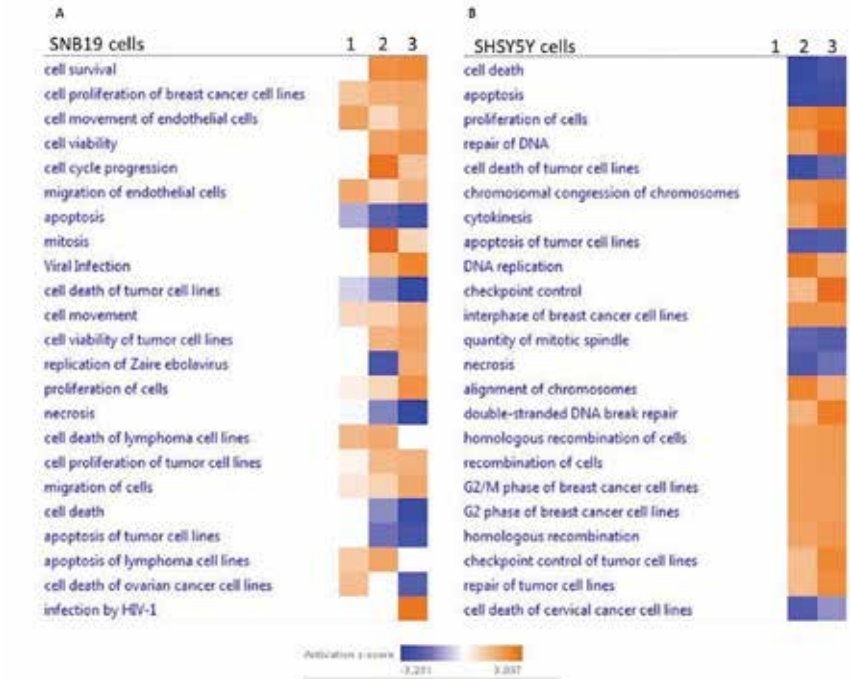

Figure 7. Comparison between the cell subgroups in functional classifications. (A) Heatmap of functional classifications associated with different SNB19 and (B) SHSY5Y cell subgroups, selected by IPA. Changes in gene expression of cellular functions for the 3 subgroup comparisons are included in this analysis. 1= scrambled control cells versus knockdown of *SDHD*. 2= scrambled control cells versus knockdown of *SDHD* and *CDKN1C*. 3= scrambled control cells versus knockdown of *SDHD* and *SLC22A18*. Double knockdown of *SDHD* and *SLC22A18* or of *SDHD* and *CDKN1C* strongly decreased apoptosis and cell death-associated gene expression in both SNB19 and SHSY5Y cells, and increased cell proliferation and cell survival-related gene expression when compared to single knockdown of *SDHD*. Orange indicates increased and blue indicates decreased Z-scores.

Protein expression of SLC22A18 and CDKN1C and somatic mutation analysis in SDHD mutant tumors without loss of chromosome 11

Most *SDHD*-linked HNPGLs show loss of the entire maternal copy of chromosome 11 (16-18), effectively preventing further genetic or functional analysis of genes and gene products found on the maternal chromosome. However, surveying 60 *SDHD* mutant tumors, we identified four (6.6%) tumors that were heterozygous (no LOH) for microsatellite markers on chromosome 11, indicating retention of chromosome 11 (Fig 8A). Reasoning that retention of maternal chromosome 11 would lead to an alternative pathway of inactivation of a bona fide *SDHD* modifier gene, we analyzed SLC22A18 and CDKN1C protein loss in all 60 tumors by IHC. Interestingly, four tumors with retention of chromosome 11 showed similarly reduced expression levels of SLC22A18 and CDKN1C compared to tumors showing loss of chromosome 11 (Fig 8B-C).

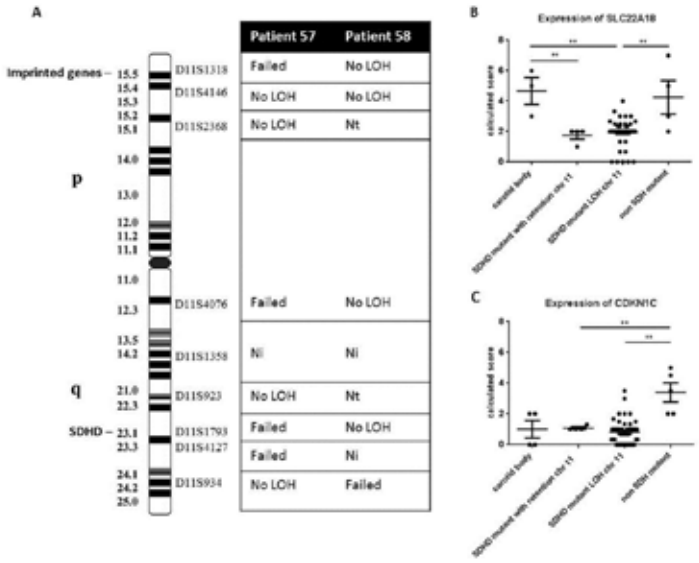

Figure 8. *SDHD* mutant tumors with retention of chromosome 11. (A) Microsatellite markers located on chromosome 11 were used for LOH analyses. Summary of LOH results for two patients, indicating no LOH (e.g. retention) of chromosome 11, which was found in a total of four patients. Nt – not tested. Ni – not informative. (B) Dot plot presenting results of immunohistochemical SLC22A18 expression demonstrating a high expression in normal post-mortem carotid bodies and non-*SDH* mutant tumors, including *RET*, *NF1* and *MEN1*-linked pheochromocytomas, which is significantly decreased in *SDHD* mutant paragangliomas with retention of chromosome 11 and loss of chromosome 11. (C) Dot plot presenting results of immunohistochemical CDKN1C expression demonstrating comparable expression levels in the 4 *SDHD*-linked tumors showing retention of chromosome 11 to *SDHD* mutant paragangliomas with LOH of chromosome 11 and significantly increased expression levels in non-*SDH* mutant tumors. Data are represented as calculated mean score ± standard error of the mean. **p<0.01.

To investigate whether somatic mutation in *CDKN1C* or *SLC22A18* might underlie protein loss, we analyzed all exons of both genes by Sanger sequencing. While no variants were found in *CDKN1C*, a missense variant was found in the coding region of *SLC22A18*, c.65G>A (p.Arg22Gln) in tumors and in normal matched DNAs in 2 cases. However, as this variant was frequent in a large population database (http://exac.broadinstitute.org), this variant is unlikely to explain *CDKN1C* or *SLC22A18* inactivation in this specific group of *SDHD* mutant PGLs/PCCs.

Discussion

Our goal in this study was to identify genes that, upon knockdown together with *SDHD*, would enhance cellular characteristics previously associated with paraganglioma/pheochromocytoma (PGL/PCC). The Hensen model postulates that tumor formation in *SDHD*-linked PGL/PCC occurs upon loss of the *SDHD* wild type gene together with a maternally-expressed tumor modifier gene probably located in the 11p15 region (17). Our evaluation of protein expression in the chief cell component of *SDHD*-mutated tumors showed that KCNQ1 and PHLDA2 were expressed and thus excluded as candidates, whereas CDKN1C, SLC22A18 and ZNF215 all showed loss of protein expression consistent with the Hensen model. The protein expression of the candidate genes H19 (noncoding RNA) and KCNQ1DN (noncoding RNA) could not be explored for obvious reasons, or due to lack of reliable antibodies (OSBPL5).

Using two distinct neural-derived cell lines, we then developed stable single and double knockdowns of *SDHD* in combination with the candidate genes *OSBPL5*, *CDKN1C*, *SLC22A18* and *ZNF215*. Consistent with earlier reports (11;23;24), we showed knockdown of *SDHD* results in a disturbed metabolism indicated by changed levels of TCA cycle metabolites and ATP in cells, and by differential gene expression of components of the oxidative response and TCA cycle. We anticipated that *SDHD* gene knockdown together with the knockdown of the relevant 11p15 tumor modifier gene would enhance PGL-related cellular characteristics compared to *SDHD* knockdown alone. Indeed, additional knockdown produced small but significant increases in cell proliferation and apoptosis resistance. Although relatively modest enhancements, similar changes found in benign, slow-growing *SDHD* mutant PGLs are also small. Large changes would in fact be intrinsically suspect. Most importantly, comparative analysis of gene expression confirmed these broader functional differences by showing decreased levels of apoptosis and increased cell proliferation compared to single knockdown.

Results from the cell line-based functional assays were further supported by the finding that *SDHD* mutant tumors with either retention or loss of chromosome 11 showed equally low levels of SLC22A18 and CDKN1C protein expression. *SDH*x mutations are associated with DNA hypermethylation and histone methylation (25), suggesting a possible mechanism underlying the lowered expression of *SLC22A18* and/or *CDKN1C* in *SDHD* mutant tumors with retention of chromosome 11.

A limitation of our *in vitro* work is that all observations were made with tumor cell lines that have already acquired genetic changes that endow them with tumorigenic growth properties. It is therefore remarkable that the knockdown of *SDHD* with or without concomitant knockdown of 11p15 candidate genes was nonetheless capable of causing additional cellular phenotypes resembling those found in primary PGLs (22). While it would have been more appropriate to perform knockdowns in normal carotid body cells, these are currently unavailable as *in vitro* cell lines. Likewise, reintroduction of *SDHD*, *SLC22A18* or *CDKN1C* into a PGL tumor cell line to revert the phenotype wasn't possible for the same reason.

The concept that *SDHD* knockdown (or knockout) alone is insufficient to trigger tumorigenesis in the carotid body is supported by work carried out in genetically engineered mice. No engineered mouse germline knockout of *Sdhb*, *Sdhc*, or *Sdhd* has developed tumors to date (26-28), and conditional tissue-specific homozygous knockout leads only to severe apoptotic loss of neuronal and chromaffin cells and early death of newborn mice (29). Starting from what we understand of SDHD PGLs in man

- the almost complete resistance to tumor development of carriers of maternally-inherited, and the loss of entire maternal chromosome 11 – we would argue that the loss of mitochondrial complex II activity in chromaffin cells can only be tolerated on a background of other genetic changes that allows them to overcome cellular lethality. Simultaneous loss of *SDHD* and *SLC22A8* and/or *CDKN1C* may create a favorable genetic landscape via a single genetic event, whole chromosome loss of chromosome 11 (30).

Loss-of-function mutations in *CDKN1C* are associated with Beckwith-Wiedemann syndrome, an overgrowth disorder related to disruption of imprinted expression of 11p15 (31). CDKN1C, encoding the cyclin-dependent kinase inhibitor 1C, inhibits cell cycle progression and may therefore lead to increased cell proliferation when lost in *SDHD* mutant PGLs. SLC22A18 is a member of a family of polyspecific transporters and multidrug resistance genes and has been reported to be a tumor suppressor candidate and a substrate for RING105, a conserved E3 ubiquitin ligase (32). Genetic mutations in *SLC22A18* are rare, with isolated reports of point mutations in a breast cancer cell line (33), a rhabdomyosarcoma cell line (34), and Wilms' tumors and lung tumors (35;36). In glioma cells, *SLC22A18* has a pro-apoptotic function and confers drug resistance (37) and more recently, downregulation of *SLC22A18* in colorectal cancer cell lines has been shown to lead to slower growth by inducing G2/M arrest (38), supporting a role for *SLC22A18* as a tumor suppressor in certain cell types. Our results showed that the combined loss of *SDHD* and *SLC22A18* leads to apoptosis resistance and may, in combination with the increased cell proliferation, result in tumor formation in *SDHD* mutant PGLs. Future studies should address this mechanism, together with the triple knockdown of these genes to assess possible synergistic interactions.

In conclusion, this study has identified two credible candidate 11p15 tumor modifier genes that may be involved in *SDHD*-linked PGL/PCC, and provides further insight into the consequences of *SDHD* knockdown in cells with a neuronal background.

References

(1) Lenders JW, Eisenhofer G, Mannelli M, Pacak K. Phaeochromocytoma. Lancet 2005 August 20;366(9486):665-75.

(2) Jansen JC, van den BR, Kuiper A, Van Der Mey AG, Zwinderman AH, Cornelisse CJ. Estimation of growth rate in patients with head and neck paragangliomas influences the treatment proposal. Cancer 2000 June 15;88(12):2811-6.

(3) Burnichon N, Briere JJ, Libe R, Vescovo L, Riviere J, Tissier F, Jouanno E, Jeunemaitre X, Benit P, Tzagoloff A, Rustin P, Bertherat J, Favier J, Gimenez-Roqueplo AP. SDHA is a tumor suppressor gene causing paraganglioma. Hum Mol Genet 2010 August 1;19(15):3011-20.

(4) Astuti D, Latif F, Dallol A, Dahia PL, Douglas F, George E, Skoldberg F, Husebye ES, Eng C, Maher ER. Gene mutations in the succinate dehydrogenase subunit SDHB cause susceptibility to familial pheochromocytoma and to familial paraganglioma. Am J Hum Genet 2001 July;69(1):49-54.

(5) Niemann S, Muller U. Mutations in SDHC cause autosomal dominant paraganglioma, type 3. Nat Genet 2000 November;26(3):268-70.

(6) Baysal BE, Ferrell RE, Willett-Brozick JE, Lawrence EC, Myssiorek D, Bosch A, van der MA, Taschner PE, Rubinstein WS, Myers EN, Richard CW, III, Cornelisse CJ, Devilee P, Devlin B. Mutations in SDHD, a mitochondrial complex II gene, in hereditary paraganglioma. Science 2000 February 4;287(5454):848-51.

(7) Hao HX, Khalimonchuk O, Schraders M, Dephoure N, Bayley JP, Kunst H, Devilee P, Cremers CW, Schiffman JD, Bentz BG, Gygi SP, Winge DR, Kremer H, Rutter J. SDH5, a gene required for flavination of succinate dehydrogenase, is mutated in paraganglioma. Science 2009 August 28;325(5944):1139-42.

(8) Koivunen P, Hirsila M, Remes AM, Hassinen IE, Kivirikko KI, Myllyharju J. Inhibition of hypoxia-inducible factor (HIF) hydroxylases by citric acid cycle intermediates - Possible links between cell metabolism and stabilization of HIF. Journal of Biological Chemistry 2007 February 16;282(7):4524-32.

(9) Pollard PJ, Briere JJ, Alam NA, Barwell J, Barclay E, Wortham NC, Hunt T, Mitchell M, Olpin S, Moat SJ, Hargreaves IP, Heales SJ, Chung YL, Griffiths JR, Dalgleish A, McGrath JA, Gleeson MJ, Hodgson SV, Poulsom R, Rustin P, Tomlinson IP. Accumulation of Krebs cycle intermediates and over-expression of HIF1alpha in tumours which result from germline FH and SDH mutations. Hum Mol Genet 2005 August 1;14(15):2231-9.

(10) Selak MA, Armour SM, MacKenzie ED, Boulahbel H, Watson DG, Mansfield KD, Pan Y, Simon MC, Thompson CB, Gottlieb E. Succinate links TCA cycle dysfunction to oncogenesis by inhibiting HIF-alpha prolyl hydroxylase. Cancer Cell 2005 January;7(1):77-85.

(11) Xiao M, Yang H, Xu W, Ma S, Lin H, Zhu H, Liu L, Liu Y, Yang C, Xu Y, Zhao S, Ye D, Xiong Y, Guan KL. Inhibition of alpha-KG-dependent histone and DNA demethylases by fumarate and succinate that are accumulated in mutations of FH and SDH tumor suppressors. Genes Dev 2012 June 15;26(12):1326-38.

(12) Dahia PL, Ross KN, Wright ME, Hayashida CY, Santagata S, Barontini M, Kung AL, Sanso G, Powers JF, Tischler AS, Hodin R, Heitritter S, Moore F, Dluhy R, Sosa JA, Ocal IT, Benn DE, Marsh DJ, Robinson BG, Schneider K, Garber J, Arum SM, Korbonits M, Grossman A, Pigny P et al. A HIF1alpha regulatory loop links hypoxia and mitochondrial signals in pheochromocytomas. PLoS Genet 2005 July;1(1):72-80.

(13) Lopez-Jimenez E, Gomez-Lopez G, Leandro-Garcia LJ, Munoz I, Schiavi F, Montero-Conde C, De Cubas AA, Ramires R, Landa I, Leskela S, Maliszewska A, Inglada-Perez L, de l, V, Rodriguez-Antona C, Leton R, Bernal C, de Campos JM, Diez-Tascon C, Fraga MF, Boullosa C, Pisano DG, Opocher G, Robledo M, Cascon A. Research resource: Transcriptional profiling reveals different pseudohypoxic signatures in SDHB and VHL-related pheochromocytomas. Mol Endocrinol 2010 December;24(12):2382-91.

(14) Kunst HP, Rutten MH, De Monnink JP, Hoefsloot LH, Timmers HJ, Marres HA, Jansen JC, Kremer H, Bayley JP, Cremers CW. SDHAF2 (PGL2-SDH5) and Hereditary Head and Neck Paraganglioma. Clin Cancer Res 2011 January 15;17(2):247-54.

(15) Van Der Mey AG, Maaswinkel-Mooy PD, Cornelisse CJ, Schmidt PH, van de Kamp JJ. Genomic imprinting in hereditary glomus tumours: evidence for new genetic theory. Lancet 1989 December 2;2(8675):1291-4.

(16) Dannenberg H, de Krijger RR, Zhao J, Speel EJ, Saremaslani P, Dinjens WN, Mooi WJ, Roth J, Heitz PU, Komminoth P. Differential loss of chromosome 11q in familial and sporadic parasympathetic paragangliomas detected by comparative genomic hybridization. Am J Pathol 2001 June;158(6):1937-42.

(17) Hensen EF, Jordanova ES, van Minderhout IJHM, Hogendoorn PCW, Taschner PEM, van der Mey AGL, Devilee P, Cornelisse CJ. Somatic loss of maternal chromosome 11 causes parent-of-origin-dependent inheritance in SDHD-linked paraganglioma and phaeochromocytoma families. Oncogene 2004 May 20;23(23):4076-83.
(18) Riemann K, Sotlar K, Kupka S, Braun S, Zenner HP, Preyer S, Pfister M, Pusch CM, Blin N. Chromosome 11 monosomy in conjunction with a mutated SDHD initiation codon in nonfamilial paraganglioma cases. Cancer Genet Cytogenet 2004 April 15;150(2):128-35.
(19) Bayley JP, Oldenburg RA, Nuk J, Hoekstra AS, van der Meer CA, Korpershoek E, McGillivray B, Corssmit EP, Dinjens WN, de Krijger RR, Devilee P, Jansen JC, Hes FJ. Paraganglioma and pheochromocytoma upon maternal transmission of SDHD mutations. BMC Med Genet 2014;15:111.
(20) Yeap PM, Tobias ES, Mavraki E, Fletcher A, Bradshaw N, Freel EM, Cooke A, Murday VA, Davidson HR, Perry CG, Lindsay RS. Molecular Analysis of Pheochromocytoma after Maternal Transmission of SDHD Mutation Elucidates Mechanism of Parent-of-Origin Effect. J Clin Endocrinol Metab 2011 September 21.
(21) van Nederveen FH, Gaal J, Favier J, Korpershoek E, Oldenburg RA, de Bruyn EM, Sleddens HF, Derkx P, Riviere J, Dannenberg H, Petri BJ, Komminoth P, Pacak K, Hop WC, Pollard PJ, Mannelli M, Bayley JP, Perren A, Niemann S, Verhofstad AA, de Bruine AP, Maher ER, Tissier F, Meatchi T, Badoual C et al. An immunohistochemical procedure to detect patients with paraganglioma and phaeochromocytoma with germline SDHB, SDHC, or SDHD gene mutations: a retrospective and prospective analysis. Lancet Oncol 2009 August;10(8):764-71.
(22) Dekker PB, Kuipers-Dijkshoorn N, Hogendoorn PC, Van Der Mey AG, Cornelisse CJ. G2M arrest, blocked apoptosis, and low growth fraction may explain indolent behavior of head and neck paragangliomas. Hum Pathol 2003 July;34(7):690-8.
(23) Imperiale A, Moussallieh FM, Sebag F, Brunaud L, Barlier A, Elbayed K, Bachellier P, Goichot B, Pacak K, Namer IJ, Taieb D. A new specific succinate-glutamate metabolomic hallmark in SDHx-related paragangliomas. PLoS One 2013;8(11):e80539.
(24) Rao JU, Engelke UF, Rodenburg RJ, Wevers RA, Pacak K, Eisenhofer G, Qin N, Kusters B, Goudswaard AG, Lenders JW, Hermus AR, Mensenkamp AR, Kunst HP, Sweep FC, Timmers HJ. Genotype-specific abnormalities in mitochondrial function associate with distinct profiles of energy metabolism and catecholamine content in pheochromocytoma and paraganglioma. Clin Cancer Res 2013 July 15;19(14):3787-95.
(25) Hoekstra AS, de Graaff MA, Briaire-de Bruijn IH, Ras C, Seifar RM, van M, I, Cornelisse CJ, Hogendoorn PC, Breuning MH, Suijker J, Korpershoek E, Kunst HP, Frizzell N, Devilee P, Bayley JP, Bovee JV. Inactivation of SDH and FH cause loss of 5hmC and increased H3K9me3 in paraganglioma/pheochromocytoma and smooth muscle tumors. Oncotarget 2015 November 17;6(36):38777-88.
(26) Letouze E, Martinelli C, Loriot C, Burnichon N, Abermil N, Ottolenghi C, Janin M, Menara M, Nguyen AT, Benit P, Buffet A, Marcaillou C, Bertherat J, Amar L, Rustin P, De RA, Gimenez-Roqueplo AP, Favier J. SDH mutations establish a hypermethylator phenotype in paraganglioma. Cancer Cell 2013 June 10;23(6):739-52.
(27) Miyazawa M, Ishii T, Kirinashizawa M, Yasuda K, Hino O, Hartman PS, Ishii N. Cell growth of the mouse SDHC mutant cells was suppressed by apoptosis throughout mitochondrial pathway. Biosci Trends 2008 February;2(1):22-30.
(28) Piruat JI, Pintado CO, Ortega-Saenz P, Roche M, Lopez-Barneo J. The mitochondrial SDHD gene is required for early embryogenesis, and its partial deficiency results in persistent carotid body glomus cell activation with full responsiveness to hypoxia. Mol Cell Biol 2004 December;24(24):10933-40.
(29) Lepoutre-Lussey C, Thibault C, Buffet A, Morin A, Badoual C, Benit P, Rustin P, Ottolenghi C, Janin M, Castro-Vega LJ, Trapman J, Gimenez-Roqueplo AP, Favier J. From Nf1 to Sdhb knockout: Successes and failures in the quest for animal models of pheochromocytoma. Mol Cell Endocrinol 2016 February 5;421:40-8.
(30) Hoekstra AS, Devilee P, Bayley JP. Models of parent-of-origin tumorigenesis in hereditary paraganglioma. Semin Cell Dev Biol 2015 July;43:117-24.
(31) Brioude F, Netchine I, Praz F, Le JM, Calmel C, Lacombe D, Edery P, Catala M, Odent S, Isidor B, Lyonnet S, Sigaudy S, Leheup B, Audebert-Bellanger S, Burglen L, Giuliano F, Alessandri JL, Cormier-Daire V, Laffargue F, Blesson S, Coupier I, Lespinasse J, Blanchet P, Boute O, Baumann C et al. Mutations of the Imprinted CDKN1C Gene as a Cause of the Overgrowth Beckwith-Wiedemann

Syndrome: Clinical Spectrum and Functional Characterization. Hum Mutat 2015 September;36(9):894-902.
(32) Yamada HY, Gorbsky GJ. Tumor suppressor candidate TSSC5 is regulated by UbcH6 and a novel ubiquitin ligase RING105. Oncogene 2006 March 2;25(9):1330-9.
(33) Gallagher E, Mc GA, Chung WY, Mc CO, Harrison M, Kerin M, Dervan PA, Mc CA. Gain of imprinting of SLC22A18 sense and antisense transcripts in human breast cancer. Genomics 2006 July;88(1):12-7.
(34) Schwienbacher C, Sabbioni S, Campi M, Veronese A, Bernardi G, Menegatti A, Hatada I, Mukai T, Ohashi H, Barbanti-Brodano G, Croce CM, Negrini M. Transcriptional map of 170-kb region at chromosome 11p15.5: identification and mutational analysis of the BWR1A gene reveals the presence of mutations in tumor samples. Proc Natl Acad Sci U S A 1998 March 31;95(7):3873-8.
(35) Lee MP, Reeves C, Schmitt A, Su K, Connors TD, Hu RJ, Brandenburg S, Lee MJ, Miller G, Feinberg AP. Somatic mutation of TSSC5, a novel imprinted gene from human chromosome 11p15.5. Cancer Res 1998 September 15;58(18):4155-9.
(36) Schwienbacher C, Angioni A, Scelfo R, Veronese A, Calin GA, Massazza G, Hatada I, Barbanti-Brodano G, Negrini M. Abnormal RNA expression of 11p15 imprinted genes and kidney developmental genes in Wilms' tumor. Cancer Res 2000 March 15;60(6):1521-5.
(37) Chu SH, Ma YB, Feng DF, Zhang H, Qiu JH, Zhu ZA. Elevated expression of solute carrier family 22 member 18 increases the sensitivity of U251 glioma cells to BCNU. Oncol Lett 2011 November;2(6):1139-42.
(38) Jung Y, Jun Y, Lee HY, Kim S, Jung Y, Keum J, Lee YS, Cho YB, Lee S, Kim J. Characterization of SLC22A18 as a tumor suppressor and novel biomarker in colorectal cancer. Oncotarget 2015 September 22;6(28):25368-80.
(39) Margetts CDE, Astuti D, Gentle DC, Cooper WN, Cascon A, Catchpoole D, Robledo M, Neumann HPH, Latif F, Maher ER. Epigenetic analysis of HIC1, CASP8, FLIP, TSP1, DCR1, DCR2, DR4, DR5, KvDMR1, H19 and preferential 11p15.5 maternal-allele loss in von Hippel-Lindau and sporadic phaeochromocytomas. Endocrine-Related Cancer 2005 March;12(1):161-72.
(40) Li LC, Dahiya R. MethPrimer: designing primers for methylation PCRs. Bioinformatics 2002 November;18(11):1427-31.
(41) Lewin J, Schmitt AO, Adorjan P, Hildmann T, Piepenbrock C. Quantitative DNA methylation analysis based on four-dye trace data from direct sequencing of PCR amplificates. Bioinformatics 2004 November 22;20(17):3005-12.
(42) Carlotti F, Bazuine M, Kekarainen T, Seppen J, Pognonec P, Maassen JA, Hoeben RC. Lentiviral vectors efficiently transduce quiescent mature 3T3-L1 adipocytes. Mol Ther 2004 February;9(2):209-17.
(43) Livak KJ, Schmittgen TD. Analysis of relative gene expression data using real-time quantitative PCR and the 2(-Delta Delta C(T)) Method. Methods 2001 December;25(4):402-8.
(44) Du P, Kibbe WA, Lin SM. lumi: a pipeline for processing Illumina microarray. Bioinformatics 2008 July 1;24(13):1547-8.
(45) Smyth GK, Michaud J, Scott HS. Use of within-array replicate spots for assessing differential expression in microarray experiments. Bioinformatics 2005 May 1;21(9):2067-75.
(46) Goeman JJ, van de Geer SA, de KF, van Houwelingen HC. A global test for groups of genes: testing association with a clinical outcome. Bioinformatics 2004 January 1;20(1):93-9.
(47) Manoli T, Gretz N, Grone HJ, Kenzelmann M, Eils R, Brors B. Group testing for pathway analysis improves comparability of different microarray datasets. Bioinformatics 2006 October 15;22(20):2500-6.
(48) Ogata H, Goto S, Sato K, Fujibuchi W, Bono H, Kanehisa M. KEGG: Kyoto Encyclopedia of Genes and Genomes. Nucleic Acids Res 1999 January 1;27(1):29-34.
(49) Hensen EF, Goeman JJ, Oosting J, Van Der Mey AG, Hogendoorn PC, Cremers CW, Devilee P, Cornelisse CJ. Similar gene expression profiles of sporadic, PGL2-, and SDHD-linked paragangliomas suggest a common pathway to tumorigenesis. BMC Med Genomics 2009;2:25.
(50) Hochberg Y, Benjamini Y. More powerful procedures for multiple significance testing. Stat Med 1990 July;9(7):811-8.
(51) Vindelov LL, Christensen IJ, Nissen NI. A detergent-trypsin method for the preparation of nuclei for flow cytometric DNA analysis. Cytometry 1983 March;3(5):323-7.
(52) Lorenz MA, Burant CF, Kennedy RT. Reducing time and increasing sensitivity in sample preparation for adherent mammalian cell metabolomics. Anal Chem 2011 May 1;83(9):3406-14.

(53) Canelas AB, ten PA, Ras C, Seifar RM, van Dam JC, van Gulik WM, Heijnen JJ. Quantitative evaluation of intracellular metabolite extraction techniques for yeast metabolomics. Anal Chem 2009 September 1;81(17):7379-89.

(54) Seifar RM, Ras C, van Dam JC, van Gulik WM, Heijnen JJ, van Winden WA. Simultaneous quantification of free nucleotides in complex biological samples using ion pair reversed phase liquid chromatography isotope dilution tandem mass spectrometry. Anal Biochem 2009 May 15;388(2):213-9.

Supplementary data

A

Marker	Location Chr 11	SHSY5Y cells		SNB19 cells	
D11S4146	3742143	195	203	195	-
D11S1758	4735970	241	243	241	-
D11S1323	6276714	202	206	201	-
D11S932	8390763	149	151	145	-
D11S4149	9130048	215	219	219	-
D11S4154	30632100	143	151	147	-
D11S4174	45 214592	failed		276	-
D11S1335	59 296727	168	170	failed	
D11S4076	61 119670	147	155	155	-
D11S4205	62 939427	failed		194	-
D11S913	65 692736	220	222	218	-
D11S2002	80 377622	239	247	233	-
D11S1358	90 005626	137	139	139	-
D11S923	100 090053	215	217	215	-
D11S1793	110 413471	121	129	failed	
D11S4127	117 181769	87	93	93	-

B

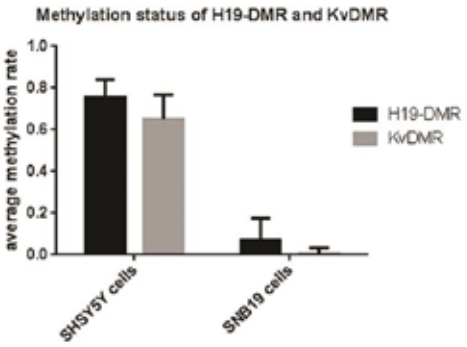

Figure S1. (A) SHSY5Y cells were heterozygous for chromosome 11 as detected by microsatellite markers, while SNB19 cells were homozygous for chromosome 11. (B) SHSY5Y cells showed an average methylation rate of 0.75 ± 0.08 for H19-DMR and 0.65 ± 0.1 for KvDMR, resulting in a ratio of 1.1. The average methylation rate for H19-DMR in SNB19 cells was 0.1 ± 0.1, while the average methylation rate for KvDMR 0.005 ± 0.03.

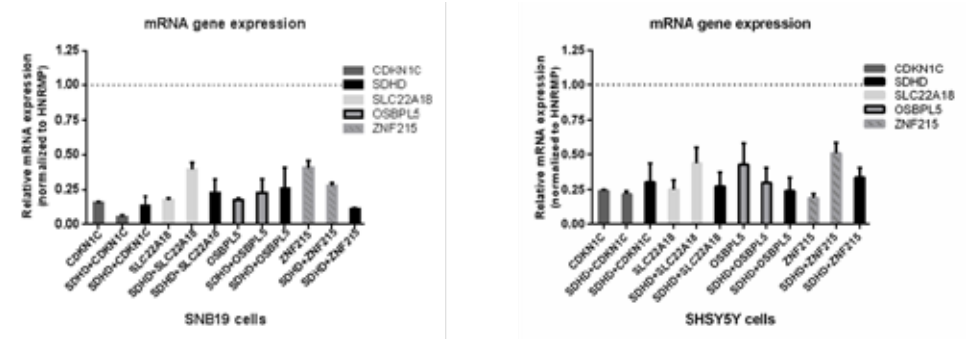

Figure S2. mRNA expression of *CDKN1C, SLC22A18, OSBPL5, ZNF215* and *SDHD* in SNB19 and SHSY5Y cells. SNB19 and SHSY5Y cells with stable knockdown of *CDKN1C, SLC22A18, OSBPL5,* or *ZNF215* using lentival shRNA and in combination with knockdown of *SDHD* results in decreased mRNA expression of *CDKN1C, SLC22A18, OSBPL5, ZNF215* and *SDHD* compared to scrambled control cells (dashed line).

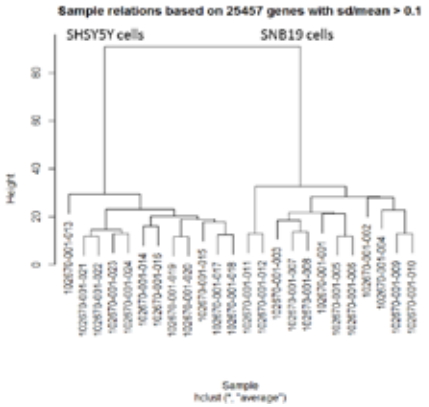

Pathway ID	KEGG pathway name	Number of genes	P-value Control vs SDHD shRNA	P-value Control vs SDHD + CDKN1C shRNA	P-value Control vs SDHD + SLC22A18 shRNA
00190	Oxidative phosphorylation	158	0,3	0,2	0,1
00020	Citrate cycle	50	0,3	0,03	0,05
00410	beta-Alanine metabolism	34	0,6	0,2	0,2
04210	Apoptosis	151	0,6	0,2	0,3
00480	Glutathione metabolism	83	0,6	0,2	0,1
00010	Glycolysis	122	0,6	0,2	0,2
05200	Pathways in cancer	601	0,6	0,2	0,3
04370	VEGF signaling pathway	130	0,6	0,2	0,3

Figure S3. Unsupervised hierarchical cluster analysis of all cells revealed two dominant expression clusters, one including all SHSY5Y samples and the other consisting of all SNB19 samples. Pathway-based analysis using the global test on pathways described in Kyoto Encyclopedia of Genes and Genomes (KEGG) revealed no significant differences between SHSY5Y cells with *SDHD* knockdown versus control cells (scrambled shRNA), whereas *SDHD+CDKN1C* knockdown or *SDHD+SLC22A18* knockdown cells compared to scrambled control cells showed significant differential expression of components of the TCA cycle.